scientific reports

Check for updates

OPEN

First-principles study on the high-pressure physical properties of orthocarbonate Ca_2CO_4

Zi-Jiang Liu[1]✉, Tian Li[1], Xiao-Wei Sun[1], Cai-Rong Zhang[2], Zhong-Li Liu[3], Ting Song[1] & Xiao-Dong Wen[1]

Orthorhombic Ca_2CO_4 is a recently discovered orthocarbonate whose high-pressure physical properties are critical for understanding the deep carbon cycle. Here, we study the structure, elastic and seismic properties of Ca_2CO_4-*Pnma* at 20–140 GPa using first-principles calculations, and compare them with the results of $CaCO_3$ polymorphs. The results show that the structural parameters of Ca_2CO_4-*Pnma* are in good agreement with the experimental results. It could be the potential host of carbon in the Earth's mantle subduction slab, and its low wave velocity and small anisotropy may be the reason why it cannot be detected in seismic observation. The thermodynamic properties of Ca_2CO_4-*Pnma* at high temperature and high pressure are obtained using the quasi-harmonic approximation method. This study is helpful in understanding the behavior of Ca-carbonate in the Earth's lower mantle conditions.

As the most important carbonate, $CaCO_3$ is transported to the deep mantle by subduction slab and plays a crucial role in the global long-term carbon cycle[1]. It is also a mineral that plays a key role in biomineralization[2]. However, $CaCO_3$ undergoes a series of phase transitions under high temperature and high pressure, forming various structures and polymorphs. So far, the predicted structures are mainly calcite, aragonite, post-aragonite, and pyroxene-like[3–9], and these structures and polymorphs have been experimentally verified[3,4,6,9–15]. Some studies also considered the reaction of calcium carbonate with MgO, SiO_2, and $MgSiO_3$[7,10,16,17], while ignoring the reaction with CaO. Previously, Al-Shemali and Boldyrev[18] mentioned the possible formation of calcium orthocarbonate Ca_2CO_4 in the $CaCO_3 + CaO$ system under high pressure. Recently, using AIRSS[19] and USPEX[20] crystal structure prediction methods, Sagatova et al.[21] discovered a new structure of calcium orthocarbonate Ca_2CO_4 (space group *Pnma*) stable at 13–50 GPa and 2000 K, the carbon atoms in this phase are fourfold coordinated, and the structure is similar to high temperature and high pressure α'_H-Ca_2SiO_4 phase[22]. Afterward, they found that Ca_2CO_4-*Pnma* was stable in the pressure and temperature range of 20–100 GPa and 1000–2000 K using the density functional theory within quasi-harmonic approximation[23]. Subsequently, Binck et al.[24] verified the results of Sagatova et al.[23] with single-crystal diffraction experiments. In addition, other alkaline earth orthocarbonates, Mg_2CO_4-*Pnma*[25], Mg_2CO_4-$P2_1/c$[25], Sr_2CO_4-*Pnma*[26], and Ba_2CO_4-*Pnma*[26] have also been predicted, of which Sr_2CO_4-*Pnma*[27] and Mg_2CO_4-$P2_1/c$[28] have been experimentally verified.

The elastic, seismic, and thermodynamic properties of Ca_2CO_4-*Pnma* under high pressure have not been investigated so far. Even the elastic constants of $CaCO_3$ polymorphs were only the experimental results of calcite[29–32] and aragonite[33,34] at ambient conditions. Using the first-principles method, Belkofsi et al. calculated the elastic constants of three calcite polymorphs(calcite-III, calcite-IIIb, calcite-VI)[35], and Huang et al. studied the elastic properties of aragonite, post-aragonite and $P2_1/c$[36]. The thermal expansion coefficient[37–42] and heat capacity[37,43–45] of calcite and aragonite were measured at ambient conditions, where there was a large difference between the fitted thermal expansion coefficient.

In this work, the structural properties, elastic properties, and seismic properties of Ca_2CO_4-*Pnma* at 20–140 GPa are studied using the first-principles calculations based on density functional theory and are compared

[1]School of Mathematics and Physics, Lanzhou Jiaotong University, Lanzhou 730070, China. [2]Department of Applied Physics, Lanzhou University of Technology, Lanzhou 730050, China. [3]Technology Innovation Center of Materials and Devices at Extreme Environment, Harbin Institute of Technology, Harbin 150001, China. ✉email: liuzj1024@hotmail.com

with the results of $CaCO_3$ polymorphs. The thermodynamic properties of Ca_2CO_4-*Pnma* are obtained by quasi-harmonic approximation method.

Methods

First-principles calculations are done with using the VASP package[46,47] with projector-augmented wave[48]. The exchange–correlation interactions adopt the Perdew-Burke-Ernzerhof functional within the generalized gradient approximation[49]. The electronic configurations of the atoms are Ca: $3s^2 3p^6 4s^2$, C: $2s^2 2p^2$, O: $2s^2 2p^4$, respectively. The cutoff energy of the plane-wave basis is set to 900 eV. The *k*-point mesh generation and data processing are obtained by vaspkit program[50]. The *k*-points mesh of Ca_2CO_4-*Pnma*, calcite, aragonite, $P2_1/c$-l, post-aragonite, $P2_1/c$-h and $C222_1$ are set to $5\times7\times4$, $9\times9\times2$, $7\times4\times6$, $7\times10\times3$, $8\times7\times8$, $8\times10\times4$, and $6\times5\times10$ using the Monkhorst–Pack scheme[51], respectively. The convergence criteria for energy and force are 1.0×10^{-8} eV and 0.02 eV/Å, respectively. Based on the optimized lattice structure, the stress–strain method is used to obtain the elastic stiffness tensor. In order to ensure the accuracy of the elastic constants of Ca_2CO_4-*Pnma*, the elastic constants of calcite and aragonite are calculated and compared with the available experimental results[32,33]. As shown in Table S1 (see Supplementary Material), the calculated results are in good agreement with the experimental results[32,33]. The thermodynamic properties are calculated using the quasi-harmonic approximation method[52] of the PHONOPY program[53,54], and the force constants are calculated using the density functional perturbation theory[55]. The supercells of aragonite and Ca_2CO_4-*Pnma* adopt $2\times2\times2$ and $2\times2\times1$ unit cells, respectively. The convergence tests of the phonon spectrum calculations of aragonite and Ca_2CO_4-*Pnma* are shown in Tables S2, S3, and Figs. S1–S8 (see Supplementary Material).

Results and discussion

Structural properties. The lattice parameters and equations of state for Ca_2CO_4-*Pnma* are presented in Fig. 1. It is found that the calculated results are in good agreement with the available experimental[24] and previous theoretical results[21,24], indicating the validity of the structure. The sensitivity of the axis to compression is c > b > a. The unit-cell volume at 0 GPa is 303.38 Å^3 and the bulk modulus and its first pressure derivative are $K_0 = 113.40$ GPa and $K_0' = 4.00$ by fitting the third-order Birch–Murnaghan equation, respectively, which are consistent with the results ($V_0 = 302.0(3)$ Å^3, $K_0 = 108(1)$ GPa, and $K_0' = 4.43(3)$) of Binck et al.[24].

In order to better understand the elastic and seismic properties of Ca_2CO_4-*Pnma*, the candidate $CaCO_3$ structures (aragonite, $P2_1/c$-l, post-aragonite, $P2_1/c$-h, $C222_1$, '–l = low pressure', '–h = high pressure') in the Earth's mantle are considered. The relative stabilities of the $CaCO_3$ polymorphs considered in this work are evaluated from their enthalpies. According to Fig. S9 (see Supplementary Material), $P2_1/c$-l stabilizes above 30 GPa and retains its stability up to 46 GPa, while $P2_1/c$-h stabilizes above 75 GPa and retains its stability up to at least 140 GPa, which are consistent with the experimental and previous theoretical results[3,5]. $CaCO_3$-$C222_1$ above 137 GPa is stable relative to post-aragonite, but this does not make any sense[5,56]. Because in this interval, the modification $P2_1/c$-h is more favorable. For comparison with calcium orthocarbonate, four modifications of $CaCO_3$ must be considered, namely aragonite (20–35 GPa), $P2_1$/c-l (35–45 GPa), post-aragonite (45–75 GPa) and $P2_1$/c-h (75–140 GPa).

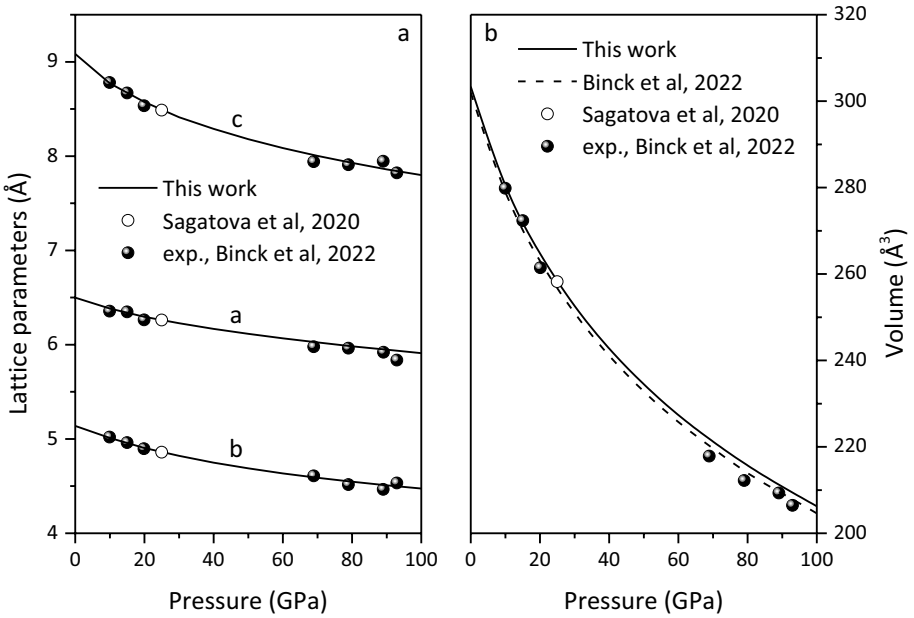

Figure 1. Lattice parameters (**a**) and equation of state (**b**) for Ca_2CO_4-*Pnma*.

Elastic properties. The calculated elastic constants of Ca_2CO_4-*Pnma* are shown in Fig. 2 and Table 1. Within the studied pressure range, $c_{11} > c_{22} > c_{33}$, indicating that compression is easier along the c-axis than along the a- and b-axes. These results are consistent with those of Fig. 1, where the lattice parameter c decreases faster than the lattice parameters a and b with increasing pressure. The calculated elastic constants of $CaCO_3$ polymorphs are shown in Figs. S10–S13 and Tables S4–S7 (see Supplementary Material), respectively. Therefore, we believe that the calculated elastic constants are correct, but experimental verification is required.

The bulk modulus (B) and shear modulus (G) of Ca_2CO_4-*Pnma* can be obtained by the Voigt[57]-Reuss[58]-Hill[59] scheme. As can be seen from Fig. 3 and Table 1, B is greater than G, indicating that with the change of volume, Ca_2CO_4-*Pnma* is more and more difficult to be compressed, and G is the main factor for the deformation of

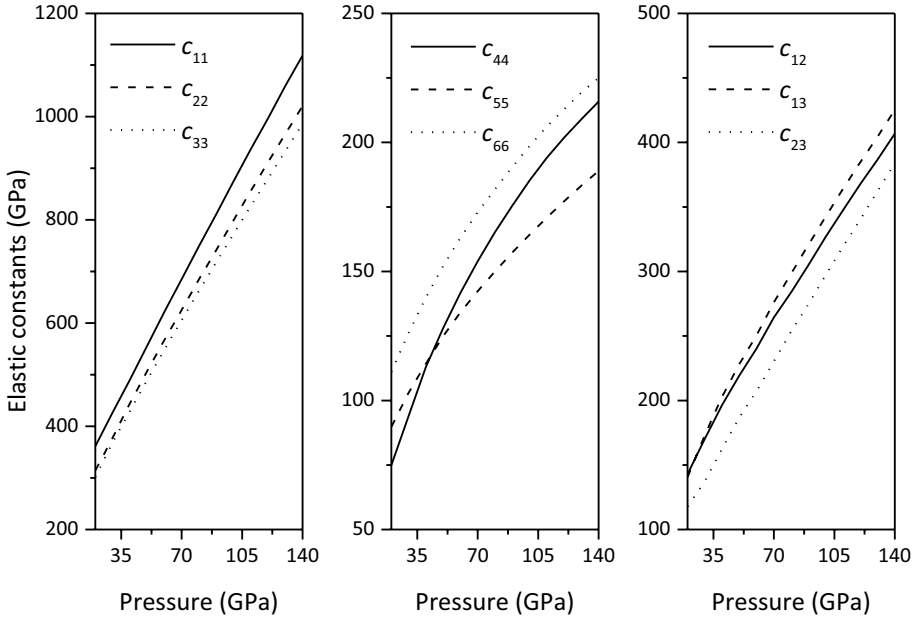

Figure 2. Elastic constants of Ca_2CO_4-*Pnma* at 20–140 GPa.

	20 GPa	30 GPa	40 GPa	50 GPa	60 GPa	70 GPa	80 GPa	90 GPa	100 GPa	110 GPa	120 GPa	130 GPa	140 GPa
c_{11}	361.283	426.524	490.296	556.045	621.896	684.963	749.298	810.915	874.479	936.647	996.922	1059.656	1118.588
c_{12}	142.903	170.233	196.570	219.457	240.398	264.397	283.931	305.062	326.853	347.379	367.839	386.722	406.809
c_{13}	140.540	173.079	203.134	228.336	250.733	276.075	298.478	320.722	342.530	364.008	384.721	404.475	425.289
c_{22}	314.362	377.291	444.437	507.012	567.550	625.190	684.971	741.163	799.215	855.726	911.686	966.326	1020.541
c_{23}	117.833	137.297	162.724	187.110	207.260	230.312	253.654	274.638	297.230	319.306	340.273	362.320	383.865
c_{33}	301.281	368.295	429.494	489.713	548.568	605.510	662.449	717.991	772.260	826.578	880.161	933.167	985.928
c_{44}	74.957	93.965	113.098	128.101	141.698	153.927	165.287	175.513	185.229	194.043	201.866	208.987	215.810
c_{55}	89.751	103.061	114.329	124.943	134.165	142.370	150.016	157.360	164.243	170.868	177.235	183.270	188.939
c_{66}	111.098	126.179	139.981	152.131	163.026	172.986	181.902	190.442	198.647	206.156	212.864	219.362	225.041
B	196.536	235.754	275.387	312.507	347.169	382.951	417.622	451.158	485.375	518.821	551.486	583.879	616.188
G	92.673	110.033	126.298	141.490	156.085	168.905	181.766	193.779	205.489	216.704	227.359	237.785	247.508
A_{100}	0.786	0.8377	0.881	0.870	0.847	0.834	0.811	0.791	0.770	0.750	0.729	0.706	0.688
A_{010}	0.945	0.8753	0.834	0.803	0.765	0.740	0.714	0.692	0.672	0.655	0.638	0.624	0.610
A_{001}	1.1400	1.0893	1.034	0.975	0.920	0.886	0.840	0.809	0.779	0.751	0.726	0.701	0.679
V_P	9.039	9.650	10.191	10.644	11.032	11.389	11.715	12.008	12.288	12.547	12.786	13.011	13.224
V_S	4.863	5.176	5.436	5.656	5.849	6.002	6.148	6.275	6.392	6.499	6.595	6.684	6.763
A_P	11.5	10.1	8.6	8.4	8.6	8.6	8.8	9.2	9.6	10.0	10.5	11.0	11.4
A_S	19.61	14.71	10.65	10.41	12.44	13.77	15.83	17.28	18.81	20.29	21.67	23.18	24.41

Table 1. Calculated elastic constants (c_{ij} , in GPa), elastic modulus (B and G, in GPa), elastic anisotropy (A_{100}, A_{010}, and A_{001}), and wave velocities(V_P and V_S, in km/s), and seismic anisotropy (A_P and A_S, in %) of Ca_2CO_4-*Pnma*.

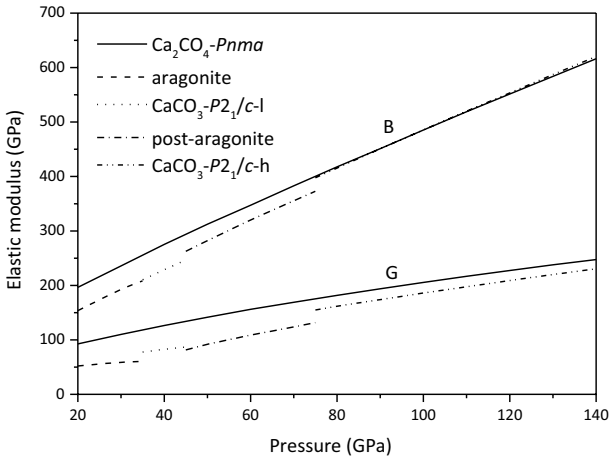

Figure 3. Bulk modulus B and shear modulus G of Ca_2CO_4-*Pnma* and $CaCO_3$ polymorphs.

Ca_2CO_4-*Pnma*. The B and G of Ca_2CO_4-*Pnma* at < 75 GPa are larger than those of $CaCO_3$ polymorphs. The B of Ca_2CO_4-*Pnma* at 75–140 GPa is equal to that of $P2_1/c$-*h*, and the G is slightly larger and almost parallel.

In order to evaluate the elastic anisotropy of Ca_2CO_4-*Pnma*, we adopt the scheme of Ravindran et al.[60]. The shear anisotropic factors of A_{100} in (100) plane, A_{010} in (010) plane, and A_{001} in (001) plane can be obtained from the following expression:

$$A_{100} = \frac{4c_{44}}{c_{11} + c_{33} - 2c_{13}} \tag{1}$$

$$A_{010} = \frac{4c_{55}}{c_{22} + c_{33} - 2c_{23}} \tag{2}$$

$$A_{001} = \frac{4c_{66}}{c_{11} + c_{22} - 2c_{12}} \tag{3}$$

The variation of shear anisotropic factors A_{100}, A_{010} and A_{001} of Ca_2CO_4-*Pnma* with pressure is displayed in Fig. 4 and Table 1. A_{010} and A_{001} gradually decrease with increasing pressure, A_{100} first increases with the increase of pressure, and then gradually decreases at > 40 GPa. It can also be found that the elastic anisotropy of Ca_2CO_4-*Pnma* in the lower mantle conditions is very small, and the anisotropy of the (010) plane between [101] and [001] directions is the smallest.

The compressional and shear wave velocities of minerals can be calculated from the elastic constants and densities. The compressional (V_P) and shear (V_S) wave velocities of Ca_2CO_4-*Pnma* and $CaCO_3$ polymorphs can be obtained from the Navier's equations[61]:

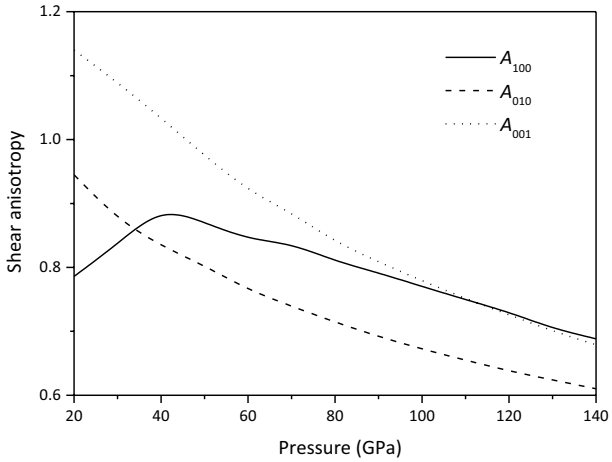

Figure 4. Shear anisotropic factors of Ca_2CO_4-*Pnma*.

$$V_P = \sqrt{\frac{3B + 4G}{3\rho}}, \quad V_S = \sqrt{\frac{G}{\rho}} \tag{4}$$

The densities and wave velocities of Ca_2CO_4-*Pnma*, $CaCO_3$ polymorphs and the Preliminary Reference Earth Model (PREM)[62] are displayed in Fig. 5 and Table 1. From Fig. 5a, it is found that the densities of Ca_2CO_4-*Pnma* in the lower mantle is less than those of PREM, and greater than those of $CaCO_3$ polymorphs. As shown in Fig. 5b, the V_P and V_S of $CaCO_4$-*Pnma* and $CaCO_3$ polymorphs are lower than those of PREM, and the V_P and V_S of Ca_2CO_4-*Pnma* are greater than those of $P2_1/c$-l and post-aragonite, which are almost the same as those of $P2_1/c$-h. The wave velocities in various crystallographic directions can be obtained by solving the Christoffel equation $\left|C_{ijkl}n_jn_l - \rho V^2\delta_{ik}\right| = 0$[63]. Figure 6 shows the wave velocities of Ca_2CO_4-*Pnma* along different crystallization directions at various pressures. The V_P of Ca_2CO_4-*Pnma* propagates the fastest in the [100] direction. The shear fast-wave velocity propagates the slowest in the [001] direction. With the increase of pressure, the propagation in the [100] and [010] directions become slower. The shear slow-wave velocity in [100] direction propagates more and more slowly as pressure increases.

The anisotropy A_P of the compressional waves and the polarization anisotropy A_S of the shear waves are defined as[65]:

$$A_P = \frac{V_{P,\max} - V_{P,\min}}{V_{P,aggregate}} \times 100\% \tag{5}$$

$$A_S = \frac{|V_{S1} - V_{S2}|_{\max}}{V_{S,aggregate}} \times 100\% \tag{6}$$

Figure 7 and Table 1 show the A_P and A_S of Ca_2CO_4-*Pnma* and $CaCO_3$ polymorphs. It can be seen that the seismic anisotropy A_P and A_S of Ca_2CO_4-*Pnma* are less than those of $CaCO_3$ polymorphs, and decrease with the increase of pressure, and gradually increase at > 45 GPa. The nonlinear dependence of seismic anisotropy on pressure can be attributed to the nonlinear pressure sensitivity of the wave velocity, which is caused by the nonlinear pressure dependence of its elastic modulus, especially the shear modulus.

The seismic properties of Ca_2CO_4-*Pnma* indicate that it could be the potential host of carbon in the subduction slab and coexists with $CaCO_3$ polymorphs, as suggested by Sagatova et al.[21,23]. It was also verified by Binck et al.[24]. The low wave velocity and small anisotropy of Ca_2CO_4-*Pnma* may be one of the reasons why it is impossible to detect the presence of carbonate in the lower mantle during the seismic observation of the subduction slab.

Thermodynamic properties. The thermodynamic parameters of minerals are a prerequisite for deriving the thermal state of the Earth's interior. In order to obtain the variation of thermodynamic parameters of Ca_2CO_4-*Pnma* with temperature and pressure, we first verify the constant pressure heat capacity C_P of aragonite at 0 GPa, and find that the calculated results are in good agreement with the experimental results[44](Fig. 8). On this basis, the predicted heat capacity and thermal expansion coefficient α of Ca_2CO_4-*Pnma* are shown in Figs. 9 and 10, respectively.

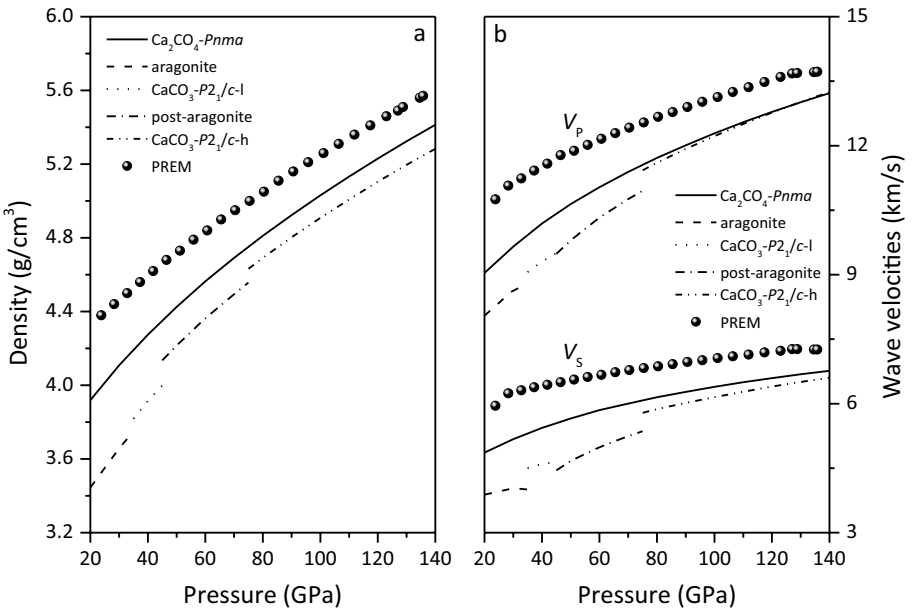

Figure 5. Densities (**a**) and wave velocities (**b**) of Ca_2CO_4-*Pnma*, $CaCO_3$ polymorphs and PREM.

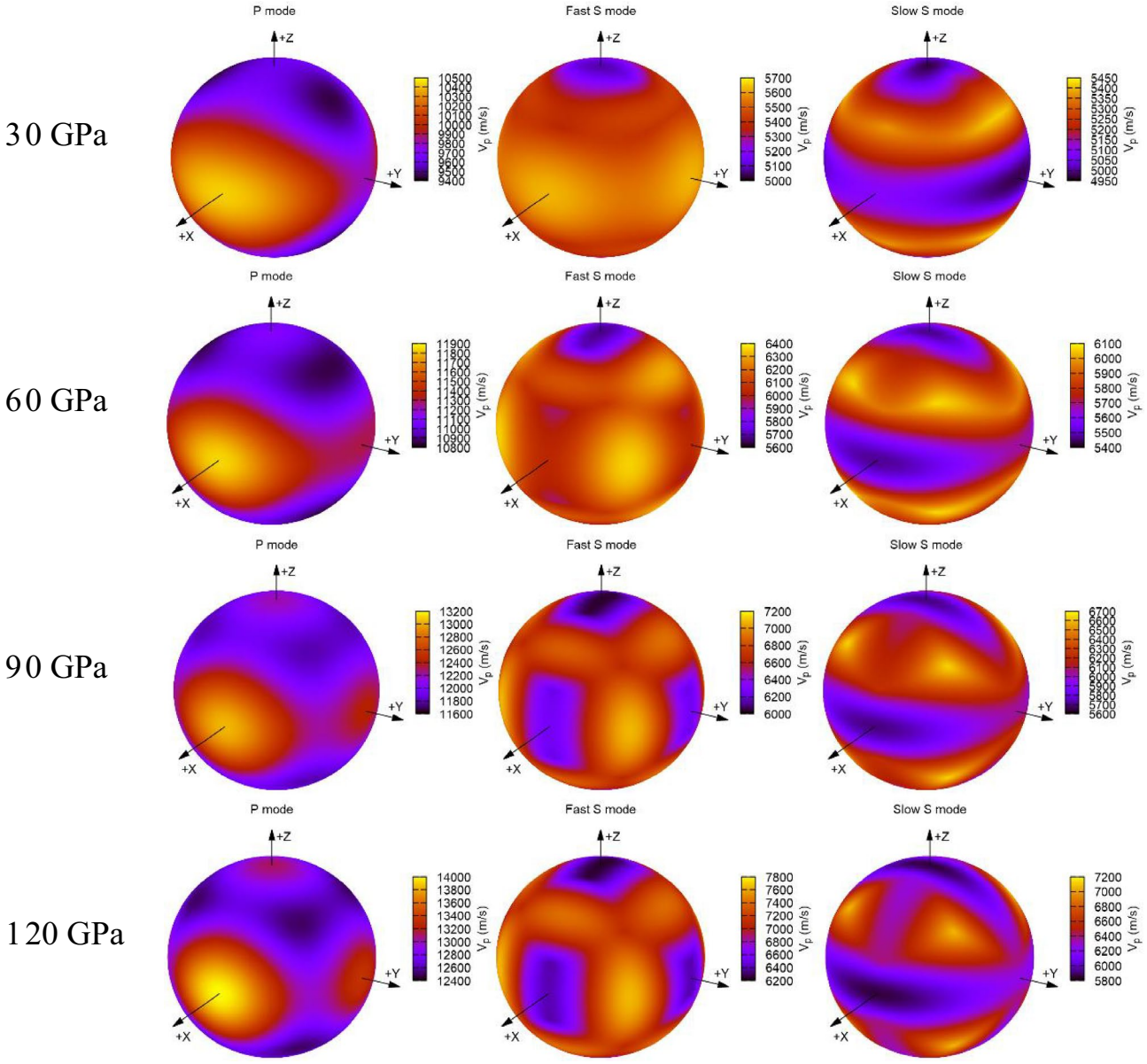

Figure 6. Wave velocities of Ca_2CO_4-*Pnma* along different crystallization directions at various pressures. Made using the AWESoMe program[64].

Figure 9 shows that the constant capacity heat capacity C_V increases sharply with increasing temperature at low temperatures. Due to the suppression of non-harmonic effects under high pressure, the constant volume heat capacity C_V under high pressure and high temperature is very close to the Dulong Petit limit. The constant pressure heat capacity C_P is very close to the constant capacity heat capacity C_V. In addition, the effects of temperature and pressure on constant capacity heat capacity C_V and constant pressure heat capacity C_P are opposite, and the impact of temperature is more noteworthy.

It can be seen from Fig. 10 that thermal expansion coefficient α at low temperature increases rapidly with the increase of temperature and tends to flatten rapidly with the increase of temperature. With the increase of pressure, the thermal expansion coefficient α decreases rapidly, and the influence of temperature becomes less and less obvious, resulting in linear high temperature behavior.

Conclusions

On the basis of the determination of the stability for $CaCO_3$ polymorphs in the lower mantle conditions and the verification of the structural parameters of Ca_2CO_4-*Pnma*, we study the elastic, seismic and thermodynamic properties of Ca_2CO_4-*Pnma*, and compared the results with those of $CaCO_3$ polymorphs. The research shows that the densities of Ca_2CO_4-*Pnma* in the lower mantle are greater than those of $CaCO_3$ polymorphs, and the seismic anisotropies are less than those of $CaCO_3$ polymorphs. The wave velocities of Ca_2CO_4-*Pnma* and $CaCO_3$ polymorphs are relatively low, and the wave velocities of Ca_2CO_4-*Pnma* and $CaCO_3$-$P2_1/c$-h are almost the same.

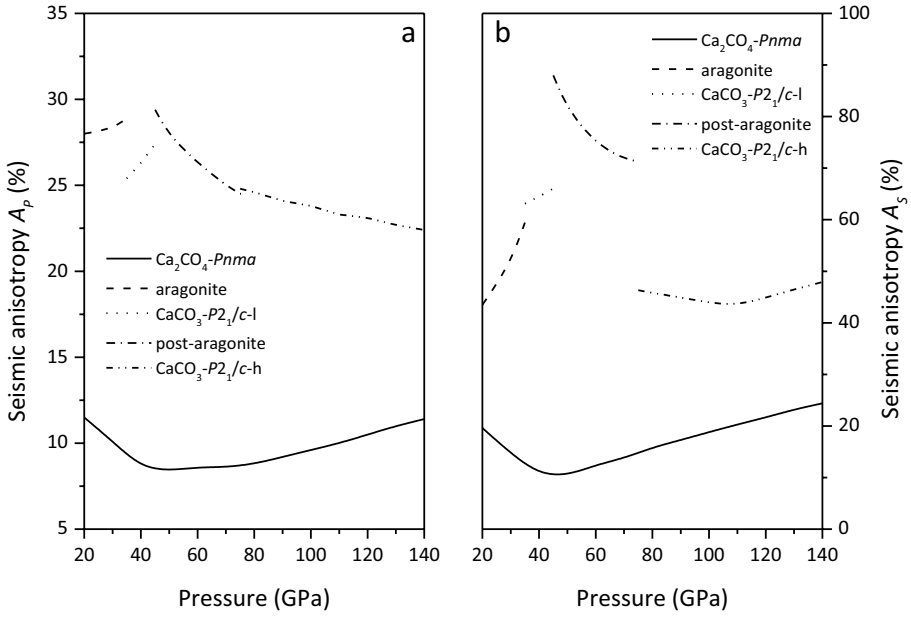

Figure 7. Seismic anisotropy A_P (**a**) and A_S (**b**) of Ca_2CO_4-*Pnma* and $CaCO_3$ polymorphs.

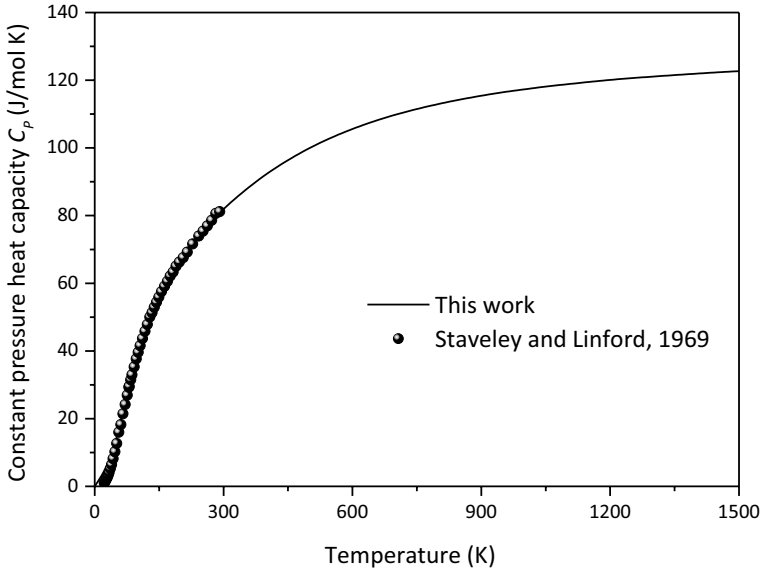

Figure 8. Constant pressure heat capacity C_P of aragonite at 0 GPa.

This means that the presence of carbonate in the lower mantle is unlikely to be detected by seismic observations of subducted slab. By verifying the constant pressure heat capacity of aragonite at 0 GPa, the thermodynamic properties of Ca_2CO_4-*Pnma* at high temperature and high pressure are calculated using the quasi-harmonic approximation method. The results of this study are helpful to better understand the behavior of calcium carbonate in the lower mantle conditions.

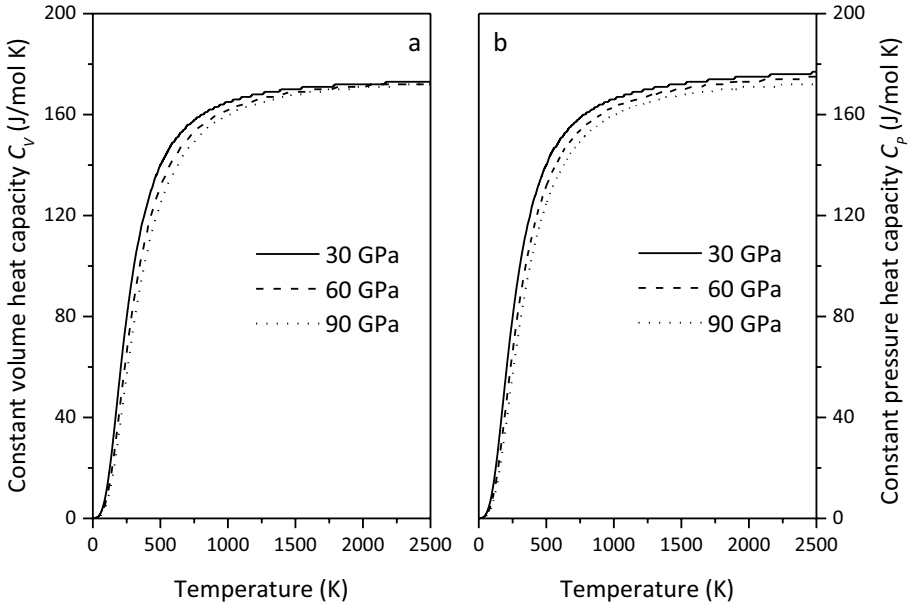

Figure 9. Constant volume heat capacity C_V (**a**) and constant pressure heat capacity C_P (**b**) of Ca_2CO_4-*Pnma* at various pressures.

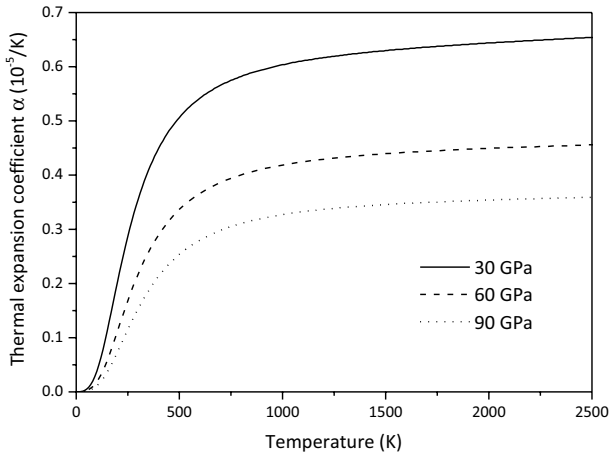

Figure 10. Thermal expansion coefficient α of Ca_2CO_4-*Pnma* at various pressures.

Data availability

The datasets used and/or analyzed during the current study available from the corresponding author on reasonable request.

Received: 16 April 2023; Accepted: 11 July 2023
Published online: 14 July 2023

References

1. Gao, J., Wu, X., Yuan, X. & Su, W. Fate of carbonates in the Earth's mantle (10–136 GPa). *Front. Earth Sci.* **10**, 837775 (2022).
2. Lowenstam, H. A. & Weiner, S. *On Biomineralization* (Oxford University Press, 1989).
3. Gavryushkin, P. N. *et al.* Aragonite-II and $CaCO_3$-VII: New high-pressure, high-temperature polymorphs of $CaCO_3$. *Cryst. Growth Des.* **17**, 6291–6296 (2017).
4. Oganov, A. R., Glass, C. W. & Ono, S. High-pressure phases of $CaCO_3$: Crystal structure prediction and experiment. *Earth Planet. Sci. Lett.* **241**, 95–103 (2006).
5. Pickard, C. J. & Needs, R. J. Structures and stability of calcium and magnesium carbonates at mantle pressures. *Phys. Rev. B* **91**, 104101 (2015).
6. Smith, D. *et al.* Postaragonite phases of $CaCO_3$ at lower mantle pressures. *Phys. Rev. Mater.* **2**, 013605 (2018).

7. Zhang, Z. G., Mao, Z., Liu, X., Zhang, Y. G. & Brodholt, J. Stability and reactions of $CaCO_3$ polymorphs in the Earth's deep mantle. *J. Geophys. Res.* **123**, 6491–6500 (2018).
8. Gavryushkin, P. N., Sagatov, N., Belonoshko, A. B., Banaev, M. V. & Litasov, K. D. Disordered aragonite: The new high-pressure, high-temperature phase of $CaCO_3$. *J. Phys. Chem. C* **124**, 26467–26473 (2020).
9. Bayarjargal, L., Fruhner, C. J., Schrodt, N. & Winkler, B. $CaCO_3$ phase diagram studied with Raman spectroscopy at pressures up to 50 GPa and high temperatures and DFT modeling. *Phys. Earth Planet. Inter.* **281**, 31–45 (2018).
10. Li, X. *et al.* New high-pressure phase of $CaCO_3$ at the topmost lower mantle: Implication for the deep-mantle carbon transportation. *Geophys. Res. Lett.* **45**, 1355–1360 (2018).
11. Ono, S., Kikegawa, T., Ohishi, Y. & Tsuchiya, J. Post-aragonite phase transformation in $CaCO_3$ at 40 GPa. *Am. Mineral.* **90**, 667–671 (2005).
12. Lobanov, S. S. *et al.* Raman spectroscopy and x-ray diffraction of sp^3 $CaCO_3$ at lower mantle pressures. *Phys. Rev. B* **96**, 104101 (2017).
13. Ono, S., Kikegawa, T. & Ohishi, Y. High-pressure transition of $CaCO_3$. *Am. Mineral.* **92**, 1246–1249 (2007).
14. Lv, M., Liu, J., Greenberg, E., Prakapenka, V. & Dorfman, S. Thermal equation of state of post-aragonite $CaCO_3$-Pmmn. *Am. Mineral.* **105**, 1365–1374 (2020).
15. Druzhbin, D., Rashchenko, S. V., Shatskiy, A. & Crichton, W. A. New high-pressure and high-temperature $CaCO_3$ polymorph. *ACS Earth Space Chem.* **6**, 1506–1513 (2022).
16. Seto, Y., Hamane, D., Nagai, T. & Fujino, F. Fate of carbonates within oceanic plates subducted to the lower mantle, and a possible mechanism of diamond formation. *Phys. Chem. Miner.* **35**, 223–229 (2008).
17. Drewitt, J. W. E. *et al.* The fate of carbonate in oceanic crust subducted into earth's lower mantle. *Earth Planet. Sci. Lett.* **511**, 213–222 (2019).
18. Al-Shemali, M. & Boldyrev, A. I. Search for ionic orthocarbonates: Ab initio study of Na_4CO_4. *J. Phys. Chem. A* **106**, 8951–8954 (2002).
19. Pickard, C. J. & Needs, R. J. Ab initio random structure searching. *J. Phys.: Condens Matter* **23**, 053201 (2011).
20. Oganov, A. R. & Glass, C. W. Crystal structure prediction using ab initio evolutionary techniques: Principles and applications. *J. Chem. Phys.* **124**, 244704 (2006).
21. Sagatova, D., Shatskiy, A., Sagatov, N., Gavryushkin, P. N. & Litasov, K. D. Calcium orthocarbonate, Ca_2CO_4-*Pnma*: A potential host for subducting carbon in the transition zone and lower mantle. *Lithos* **370–371**, 105637 (2020).
22. Belmonte, D., Ottonello, G. & Zuccolini, M. V. Ab initio-assisted assessment of the CaO–SiO_2 system under pressure. *Calphad* **59**, 12–30 (2017).
23. Sagatova, D. N., Shatskiy, A. F., Gavryushkin, P. N., Sagatov, N. E. & Litasov, K. D. Stability of Ca_2CO_4-*Pnma* against the main mantle minerals from ab initio computations. *ACS Earth Space Chem.* **5**, 1709–1715 (2021).
24. Binck, J. *et al.* Synthesis of calcium orthocarbonate, Ca_2CO_4-*Pnma* at *P-T* conditions of Earth's transition zone and lower mantle. *Am. Mineral.* **107**, 336–342 (2022).
25. Gavryushkin, P. N., Sagatova, D. N., Sagatov, N. & Litasov, K. D. Formation of Mg-orthocarbonate through the reaction $MgCO_3$+MgO=Mg_2CO_4 at Earth's lower mantle *P–T* conditions. *Cryst. Growth Des.* **21**, 2986–2992 (2021).
26. Gavryushkin, P. N., Sagatova, D. N., Sagatov, N. & Litasov, K. D. Orthocarbonates of Ca, Sr, and Ba-the appearance of sp^3-hybridized carbon at a low pressure of 5 GPa and dynamic stability at ambient pressure. *ACS Earth Space Chem.* **5**, 1948–1957 (2021).
27. Spahr, D. *et al.* Tetrahedrally coordinated sp^3-hybridized carbon in Sr_2CO_4 orthocarbonate at ambient conditions. *Inorg. Chem.* **60**, 5419–5422 (2021).
28. Gavryushkin, P. N. *et al.* First experimental synthesis of Mg orthocarbonate by the $MgCO_3$+MgO=Mg_2CO_4 reaction at pressures of the Earth's lower mantle. *JETP Lett.* **116**, 477–484 (2022).
29. Chen, C.-C., Lin, C.-C., Liu, L.-G., Sinogeikin, S. V. & Bass, J. D. Elasticity of single-crystal calcite and rhodochrosite by Brillouin spectroscopy. *Am. Mineral.* **86**, 1525–1529 (2001).
30. Dandekar, D. P. Variation in the elastic constants of calcite with temperature. *J. Appl. Phys.* **39**, 3694–3699 (1968).
31. Dandekar, D. P. Pressure dependence of the elastic constants of calcite. *Phys. Rev.* **172**, 873–877 (1968).
32. Hearmon, R. F. S., *The elastic constants of crystals and other anisotropic materials*. K. H. Hellwege, A. M. Hellwege, Eds., Landolt-Bornstein Tables,III/11 (Springer-Verlag, 1979).
33. Liu, L.-G., Chen, C.-C., Lin, C.-C. & Yang, Y.-J. Elasticity of single-crystal aragonite by Brillouin spectroscopy. *Phys. Chem. Minerals* **32**, 97–102 (2005).
34. Hearmon, R. F. S. The elastic constants of anisotropic minerals. *Rev. Mod. Phys.* **8**, 409–440 (1946).
35. Belkofsi, R., Adjaoud, O. & Belabbas, I. Pressure induced phase transitions and elastic properties of $CaCO_3$ polymorphs: a density functional theory study. *Modell. Simul. Mater. Sci. Eng.* **26**, 065004 (2018).
36. Huang, D. *et al.* Elastic properties of $CaCO_3$ high pressure phases from first principles. *Chin. Phys. B* **26**, 089101 (2017).
37. Litasov, K. D. *et al. P-V-T* equation of state of $CaCO_3$ aragonite to 29 GPa and 1673 K: In situ X-ray diffraction study. *Phys. Earth Planet. Inter.* **265**, 82–91 (2017).
38. Palaich, S. E. M. *et al.* High-pressure compressibility and thermal expansion of aragonite. *Am. Mineral.* **101**, 1651–1658 (2016).
39. Li, Y. *et al. P-V-T* equation of state and high-pressure behavior of $CaCO_3$ aragonite. *Am. Mineral.* **100**, 2323–2329 (2015).
40. Antao, S. M. & Hassan, I. Temperature dependence of the structural parameters in the transformation of aragonite to calcite, as determined from in situ synchrotron powder X-ray-diffraction data. *Can. Mineral.* **48**, 1225–1236 (2010).
41. Matas, J., Gillet, P., Ricard, Y. & Martinez, I. Thermodynamic properties of carbonates at high pressures from vibrational modelling. *Eur. J. Mineral.* **12**, 703–720 (2000).
42. Martinez, I., Zhang, J. & Reeder, R. J. In situ X-ray diffraction of aragonite and dolomite at high pressure and high temperature: Evidence for dolomite breakdown to aragonite and magnesit. *Am. Mineral.* **81**, 611–624 (1996).
43. Lucas, A., Mouallem-Bahout, M., Carel, C., Gaude, J. & Matecki, M. Thermal expansion of synthetic aragonite condensed review of elastic properties. *J. Solid State Chem.* **146**, 73–78 (1999).
44. Staveley, L. A. K. & Linford, R. G. The heat capacity and entropy of calcite and aragonite, and their interpretation. *J. Chem. Thermodyn.* **1**, 1–11 (1969).
45. Robie, R. A., Hemingway, B. S. & Fisher, J. R., *Thermodynamic properties of minerals and related substances at 298.15 K and 1 bar (10^5 pascals) pressure and at higher temperatures*. Bulletin (U.S. G.P.O, 1978).
46. Kresse, G. & Furthmüller, J. Efficient iterative schemes for ab initio total-energy calculations using a plane-wave basis set. *Phys. Rev. B* **54**, 11169–11186 (1996).
47. Kresse, G. & Furthmüller, J. Efficiency of ab-initio total enery calculations for metals and semiconductors using a plane-wave basis set. *Comput. Mater. Sci.* **6**, 15–50 (1996).
48. Blöchl, P. E. Projector augmented-wave method. *Phys. Rev. B* **50**, 17953–17979 (1994).
49. Perdew, J. P., Burke, K. & Ernzerhof, M. Generalized gradient approximation made simple. *Phys. Rev. Lett.* **77**, 3865–3868 (1996).
50. Wang, V., Xu, N., Liu, J. C., Tang, G. & Geng, W. T. VASPKIT: A user-friendly interface facilitating high-throughput computing and analysis using VASP code. *Comput. Phys. Commun.* **267**, 108033 (2021).
51. Monkhorst, H. J. & Pack, J. D. Special points for Brillouin-zone integrations. *Phys. Rev. B* **13**, 5188–5192 (1976).
52. Togo, A., Chaput, L., Tanaka, I. & Hug, G. First-principles phonon calculations of thermal expansion in Ti_3SiC_2, Ti_3AlC_2, and Ti_3GeC_2. *Phys. Rev. B* **81**, 174301 (2010).

53. Togo, A. & Tanaka, I. First principles phonon calculations in materials science. *Scr. Mater.* **108**, 1–5 (2015).
54. Togo, A. First-principles phonon calculations with phonopy and phono3py. *J. Phys. Soc. Jpn.* **92**, 012001 (2023).
55. Gonze, X. & Lee, C. Dynamical matrices, Born effective charges, dielectric permittivity tensors, and interatomic force constants from density-functional perturbation theory. *Phys. Rev. B* **55**, 10355–10368 (1997).
56. Yao, X., Xie, C., Dong, X., Oganov, A. R. & Zeng, Q. Novel high-pressure calcium carbonates. *Phys. Rev. B* **98**, 014108 (2018).
57. Voigt, W. *Lehrbuch der Kristallphysik-mit Ausschluß der Kristalloptik* (Vieweg+Teubner Verlag, 1966).
58. Reuss, A. Calulation of yielding mixed crystals plasticity condition for single crystals. *Z. Angew. Math. Mech.* **9**, 49–58 (1929).
59. Hill, R. The elastic behavior of a crystalline aggregate. *Proc. Phys. Soc. Lond.* **65A**, 349–354 (1952).
60. Ravindran, P. *et al.* Density functional theory for calculation of elastic properties of orthorhombic crystals: Application to $TiSi_2$. *J. Appl. Phys.* **84**, 4891–4904 (1998).
61. Anderson, O. L. A simplified method for calculating the debye temperature from elastic constants. *J. Phys. Chem. Solids* **24**, 909–917 (1963).
62. Dziewonski, A. M. & Anderson, D. L. Preliminary reference Earth model. *Phys. Earth Planet. Inter.* **25**, 297–356 (1981).
63. Every, A. G. General closed-form expressions for acoustic waves in elastically anisotropic solids. *Phys. Rev. B* **22**, 1746–1760 (1980).
64. Muñoz-Santiburcio, D. & Hernández-Laguna, A. AWESoMe 1.1: A code for the calculation of phase and group velocities of acoustic waves in homogeneous solids. *Comput. Phys. Commun.* **217**, 212–214 (2017).
65. Kiefer, B., Stixrude, L., Hafner, J. & Kresse, G. Structure and elasticity of wadsleyite at high pressures. *Am. Mineral.* **86**, 1387–1395 (2001).

Acknowledgements

This work is supported by the Industrial Support and Guidance Project of Colleges and Universities of Gansu Province (No. 2022CYZC-37), the Key Natural Science Foundation of Gansu Province (No. 20JR5RA211) and the Talent Innovation and Entrepreneurship Project of Lanzhou City (No. 2020-RC-18).

Author contributions

Z.-J.L. designed the calculations and wrote the manuscript. X.-W.S., C.-R.Z. and Z.-L.L analyzed the results. T.L., T.S. and X.-D.W. performed partial calculations. All authors reviewed the manuscript.

Competing interests

The authors declare no competing interests.

Additional information

Supplementary Information The online version contains supplementary material available at https://doi.org/10.1038/s41598-023-38604-w.

Correspondence and requests for materials should be addressed to Z.-J.L.